DOI: 10.1021/ma902637a

Macromolecules
ARTICLE

Swelling and switching kinetics of gold coated end-capped poly(*N*-isopropylacrylamide) thin films

W. Wang,[†] G. Kaune,[†] J. Perlich,[†,§] C. M. Papadakis,[†] A. M. Bivigou Koumba,[‡] A. Laschewsky,[‡] K. Schlage,[§] R. Röhlsberger,[§] S. V. Roth,[§] R. Cubitt,[⊥] and P. Müller-Buschbaum*[,†]

[†]*TU München, Physik-Department LS E13, James-Franck-Strasse 1, 85747 Garching, Germany,*
[‡]*Institut für Chemie, Potsdam Universität, Karl-Liebknecht-Strasse 24-25, 14476 Potsdam-Golm, Germany,*
[§]*Deutsches Elektronen Synchrotron DESY, Notkestr. 85, 22603 Hamburg, Germany, and*
[⊥]*Institut Laue Langevin (ILL), 6 Jules Horowitz, 38042 Grenoble, France*

Received November 30, 2009; Revised Manuscript Received January 20, 2010

ABSTRACT: Thin thermoresponsive hydrogel films of poly(*N*-isopropylacrylamide) end-capped with *n*-butyltrithiocarbonate (nbc-PNIPAM) on silicon supports with a gold layer on top, causing an asymmetric confinement, are investigated. For two different gold layer thicknesses (nominally 0.4 and 5 nm), the swelling and switching kinetics are probed with in situ neutron reflectivity. With a temperature jump from 23 to 40 °C the film is switched from a swollen into a collapsed state. For the thin gold layer this switching is faster as compared to the thick gold layer. The switching is a two-step process of water release and a subsequent structural relaxation. In swelling and deswelling cycles, aging of the films is probed. After five cycles, the film exhibits enhanced water storage capacity. Grazing-incidence small-angle X-ray scattering (GISAXS) shows that these gold coated nbc-PNIPAM films do not age with respect to the inner structure but slightly roughen at the gold surface. As revealed by atomic force microscopy, the morphology of the gold layer is changed by the water uptake and release.

1. Introduction

Environmentally responsive polymers have been widely studied over the last decades. Among the thermoresponsive polymers poly(*N*-isopropylacrylamide) (PNIPAM) is heavily investigated[1−13] and frequently used in applications.[2,14−18] PNIPAM in water exhibits a phase transition at a lower critical solution temperature (LCST), which has been investigated by a variety of experimental techniques in dilute and concentrated solutions. PNIPAM polymers are well hydrated and swollen in their hydrophilic state (below 32 °C), while they release water and collapse in the hydrophobic one (above 32 °C). PNIPAM is characterized by a very weak sensitivity of the LCST on molecular parameters such as the molecular weight and the particular value of the LCST which in water is slightly less than body temperature (at 32 °C).[2] For technical and biomedical applications such value and the insensitivity are beneficial. Therefore, PNIPAM is successfully used in various fields including microactuators and microvalves,[19] optical devices,[20] protein screening and fractionation,[21] controlled drug and gene delivery,[22] and solute separators.[23]

However, many technical applications require a mechanical stability which is offered by a PNIPAM hydrogel.[24] Instead of introducing chemical cross-links to obtain the hydrogel, physical cross-links can be generated by the use of PNIPAM-based block copolymers with a hydrophobic second block. In most cases, polystyrene (PS) was chosen as the hydrophobic, glassy block, and diblock copolymers P(S-*b*-NIPAM)[25−28] and triblock copolymers P(S-*b*-NIPAM-*b*-PS) were studied.[13,29−35] But, by adding hydrophobic, glassy units to the PNIPAM chain, the response and the LCST are affected. Moreover, the swelling ability reduces with increasing size of the PS block.[26,36,37] As a consequence, the other extreme of having only small end-groups compromises an optimal swelling capacity with a certain mechanical stability. Recently, we have investigated PNIPAM end-capped with *n*-butyltrithiocarbonate (nbc-PNIPAM).[38] This end-capped PNIPAM can be understood as the extreme of a triblock copolymer by showing an internal structure and a strong swelling even in water vapor.[38]

Regarding the response time, bulk hydrogels are slow, promoting microgels[39−42] and thin films[43−46] to be considered as better systems with shorter response times. The volume change appears much faster if the hydrogel dimensions are in the submicrometer range. In particular, thin films allow for advanced applications such as thermoresponsive surfaces, miniaturized sensor systems, and nanoswitches.[47−52] Whereas thermoresponsive surfaces make use of a change in the wetting properties, triggered by a change in temperature, miniaturized sensor systems and nanoswitches are based on the change in hydrogel film thickness, because the surface area is fixed.[38]

A simplified thin film model sensor and nanoswitch will consist of the active (sensor) layer and a metal top-layer on top of a solid support. The active layer contains PNIPAM. Such sandwich structure gives rise to an asymmetric confinement of the PNIPAM film. Although PNIPAM and the temperature responsiveness of its aqueous solutions or water-soaked films have been studied in great detail,[1−13,38] PNIPAM-based, confined polymer thin films are rarely investigated. Regardless of the polymer and metal used, an important concern in metal coatings are the interactions occurring at the metal−polymer interface, since characteristics like swelling and switching behavior could be strongly influenced by the presence of an additional interface. Related to this is the question how the polymer and the swelling and switching process influence the metal film morphology.

*Corresponding author. Telephone: +49 89 289 12451. Fax: +49 89 28912473. E-mail: muellerb@ph.tum.de.

 Published on Web 02/09/2010

In the present investigation we use nbc-PNIAPM and a gold top-layer. Central aim of this work is to probe the swelling and switching kinetics of such confined, gold coated nbc-PNIPAM films. These films are exposed to water vapor atmosphere to detect the swelling kinetics and capacity, resembling the sensor function. In addition, these films are switched by a temperature jump from a temperature well below the LCST to a temperature well above the LCST. Such jump will operate the film as a nanoswitch.

With the use of deuterated water and protonated nbc-PNIPAM we have a good contrast to detect the amount of water absorbed inside the polymer layer by using neutron reflectivity. With neutron reflectivity the density profile along the surface normal is accessed. In situ measurements allow for monitoring changes in the composition during contact with a surrounding (deuterated) water vapor. These measurements are complemented by atomic force microscopy to observe the surface morphology of the gold layer and by grazing-incidence small-angle X-ray scattering to detect lateral structures inside the nbc-PNIPAM films. We investigate two different gold layer thicknesses: A thin gold layer of 0.4 nm nominal total thickness and a thick gold layer being nominally 5 nm thick.

This article has the following structure: The introduction is followed by an Experimental Section describing the sample preparation and the experimental techniques applied. The next sections show results and discussion of the gold layer deposition and the switching kinetics caused by the temperature jump, followed by the swelling kinetics and cyclic swelling. A Conclusion ends the article.

2. Experimental Section

2.1. Materials. The polymer used is *n*-butyltrithiocarbonate end-capped poly(*N*-isopropylacrylamide), denoted nbc-PNIPAM, with a molecular weight of 39000 g mol^{-1}. The synthesis process and molecular characteristics of the polymer are described in detail elsewhere.[38] Deuterated water (D_2O) (purity 99.95%) was purchased from Deutero GmbH. 1,4-dioxane was received from Acros. Dichloromethane, ammonia solutions (NH_3, 30−33%), and hydrogen peroxide (H_2O_2, 30%) were ordered from Carl Roth GmbH. Silicon substrates (Si 100, n-type) were from Silchem.

2.2. Sample Preparation. We used precleaned silicon with a native oxide layer on the surface as substrates for the thin nbc-PNIPAM films. In the cleaning protocol,[53] the precut silicon substrates were placed in dichloromethane in an ultrasonic bath at 46 °C for 30 min and rinsed with Millipore water shortly after. Afterward, the substrates were kept for 2 h in an oxidation bath at 75 °C consisting of 1400 mL of Millipore water, 120 mL of H_2O_2, and 120 mL of NH_3 to clean the surface from organic traces and install a hydrophilic surface. Thereafter, the substrates were stored briefly in Millipore water. Directly before spin-coating the substrates were rinsed with Millipore water for at least 10 min to remove possible traces of the oxidation bath. The substrates were dried with compressed nitrogen immediately before coating. Because of this protocol, at the Si surface an oxide layer of 1 nm is present, which has a surface roughness smaller than 0.5 nm.

The initial nbc-PNIPAM films were prepared with spin-coating (2000 rpm, 30 s) from a 1,4-dioxane solution at room temperature onto these precleaned Si substrates. A film thickness of 39 nm was selected by making use of the recently determined film thickness dependence on the concentration of the solution used in the spin-coating process.[38] In a second step, the top gold layer was added by sputter deposition. For this purpose, the samples were mounted in a sputter deposition chamber,[54] and the gold deposition was performed at an argon pressure of 4×10^{-3} mbar while the deposition rate was set to 0.43 nm/min. The final, nominal gold layer thicknesses after deposition were 0.4 and 5 nm, respectively. This gold layer was investigated with AFM and neutron reflectivity measurements.

2.3. Temperature Jump Experiment. The initial dry, gold coated nbc-PNIPAM film of the desired gold layer thickness was mounted in a custom-made vapor chamber in air, thermostated to 23 °C and investigated. To prepare a swollen and equilibrated film for the temperature jump experiment, the vapor chamber was evacuated, and the water reservoir of the vapor chamber was filled with D_2O to install a saturated D_2O atmosphere. After reaching equilibrium of swelling water vapor atmosphere (230 min) the film was cycled in 7 swelling and deswelling cycles as described below. To initiate the temperature jump from 23 to 40 °C, the set up was thermostated to 40 °C and investigated with in situ neutron reflectivity (time = 0). We operated a rate of 3.1 °C/min for increasing the temperature in the setup to avoid overshooting of the temperature.

2.4. Swelling Cycle Protocol. The initial swelling process of the dry, gold coated nbc-PNIPAM film was the same as that described in the temperature jump experiment. The addition of D_2O marks the starting point of the water absorption kinetics (time = 0). Again, equilibrium of swelling was reached after 230 min and the film was fully swollen. The deswelling by removal of D_2O was initiated by pumping the vapor chamber through a vacuum pump (DIVAC 0.8 T, Leybold AG). Thus, water release from the thin film occurred, and the gold coated nbc-PNIPAM film relaxed back under vacuum to a new dry state. This deswollen film was used in the next swelling cycle as the initial dry film. To address the aging effects of the swelling in water vapor atmosphere, the swelling and deswelling cycles were repeated 7 times. Samples were investigated in situ during these cycles with neutron reflectivity and ex situ after individual cycles with the other experimental techniques.

2.5. Neutron Reflectivity and Off-Specular Scattering. The neutron scattering experiments were carried out at the D17 instrument at ILL, Grenoble, in time-of-flight (TOF) mode.[55] In TOF mode, specular and off-specular scattering data were collected. Neutrons with a broad range of wavelength λ were used simultaneously and registered as a function of their respective times of flight. The necessary pulsing of the beam was realized by a double chopper system. We selected the largest available sample−detector distance of 3.4 m. The scattered intensity was recorded on a two-dimensional (2D) detector without the movement of any motors. This absence of motor movements was crucial on the one hand for achieving a high time resolution and on the other hand for avoiding mechanically induced vibrations which might destabilize swollen films (by activation of long wavelength surface waves). Counts on the detector were registered for each spatial pixel (x, y) as a function of TOF in channels. After integration of the counts for fixed x and TOF channels along the vertical detector axis y, and the TOF to λ conversion, the scattered intensity was displayed as a function of λ and the exit angle α_f. Finally, the corrected data set $I(\alpha_f, \lambda)$ can also be transformed to $I(q_x, q_z)$ with the given (constant) incident angle α_i, where q_z denotes the wave vector component perpendicular to the surface and q_x the one in the surface in parallel to the neutron beam.

The incident angle α_i was kept constant at 0.5° during the kinetic experiments. The probed q_z range between 0.01 and 0.85 nm^{-1} was selected to cover the critical edges of protonated (Si and gold coated nbc-PNIPAM) and deuterated (D_2O) substances. Kinetic changes in the temperature jump experiment and in the swelling and deswelling cycles were probed by performing reflectivity scans every 14 s (10 s data acquisition time and 4 s data read-out time). In case of the 0.4 nm gold layer thickness 24 s (20 s data acquisition time and 4 s data read-out time) were necessary to account for the weaker scattering signal as compared to the 5 nm thick gold layer samples.

With static scattering experiments the initial gold coated nbc-PNIPAM films and the resulting deswollen gold coated nbc-PNIPAM film at the end of each cycle were additionally probed.

An increased counting time of 3600 s and a larger angular range with two fixed incident angles were operated.

All reflectivity curves were fitted with the Motofit program[56,57] with appropriate error weighting and point-by-point resolution smearing. An automated batch fit approach was taken, with all the data sets being analyzed in series. The scattering length densities of 2.07×10^{-6} Å^{-2} for Si, 3.47×10^{-6} Å^{-2} for Si oxide, 0.88×10^{-6} Å^{-2} for nbc-PNIPAM, 4.2×10^{-6} Å^{-2} for gold and 6.36×10^{-6} Å^{-2} for D_2O were obtained from initial fits. They agree with textbook values.

2.6. Grazing-Incidence Small-Angle X-ray Scattering. The grazing incidence small-angle X-ray scattering (GISAXS) measurements were performed at the synchrotron beamline BW4 at DORIS III (HASYLAB at DESY, Hamburg, Germany). Synchrotron radiation with a wavelength of $\lambda = 0.138$ nm was used. The beam shape in and out of the plane of reflection was set by two entrance cross slits. A beam size of smaller than $30 \times 20\ \mu m^2$ (horizontal × vertical) was achieved by using an assembly of beryllium compound refractive lenses.[58]

For the measurement, the sample was placed horizontally on a goniometer. The angle of incidence was set to $\alpha_i = 0.384°$ which is above the critical angle α_c of the investigated polymer (PNIPAM: 0.148°). Hence, the Yoneda peak was well separated from the specular peak on the detector, and both the sample surface and the interior of the film were probed. A 2D detector (MarCCD 165 by Mar Research, 2048 × 2048 pixels) was positioned with a sample-to-detector distance of $D = 2.165$ m behind the sample. From the recorded 2D intensity distribution, structural information on the sample was extracted from horizontal and vertical cuts (with respect to the sample surface).[59] The vertical cut at a horizontal angle of $\Psi = 0°$, corresponding to $q_y = 0$, contains information about structures perpendicular to the surface (e.g., the correlated roughness) as well as the material-specific Yoneda peaks at $\alpha_f = \alpha_c$. Horizontal cuts were performed at constant q_z and were selected according to the q_z condition ($\alpha_f = \alpha_c$). From the q_y cuts, lateral structure information (e.g., geometry, size distribution and spatial correlation) is extracted. In order to improve statistics, the intensity of q_y cuts in a narrow range of Δq_z was integrated.[59]

2.7. Optical Microscopy. The sample surfaces were investigated with optical microscopy using a Zeiss Axiotech 25H optical microscope with magnifications between 5× and 100×. A Hitachi KP-D50 CCD camera recorded the micrographs.

2.8. Atomic Force Microscopy. The surface topography of dry, gold-coated nbc-PNIPAM films was imaged with atomic force microscopy (AFM) in tapping mode condition. The measurements were carried out with an Autoprobe CP Research AFM instrument in ambient air atmosphere at room temperature. Gold coated silicon cantilevers (Ultralever cantilevers) were used. These cantilevers had a resonance frequency of 75 kHz and a spring constants of 2.1 N/m. The used tips had an asymptotic conical shape with a high aspect ratio and a curvature radius of 10 nm which is small as compared to the measured structures. To improve the accuracy of the AFM height and lateral information, calibration was performed with calibration standards.

3. Results and Discussion of Gold Layer Deposition

In order to have a well-defined model system for an asymmetrically confined hydrogel film and thus a basic model system for thin film sensors and nanoswitches, the thin nbc-PNIPAM films on silicon supports are capped with a top gold layer via sputter deposition. We select two different nominal gold layer thicknesses, a small one (0.4 nm) and a big one (5 nm). The nbc-PNIPAM film thickness is kept fixed (39 nm) for both types of top layers. These initial films are characterized with neutron reflectivity and atomic force microscopy to detect the density profile along the surface normal and the surface morphology of the gold.

In Figure 1 the neutron reflectivity data are displayed together with model fits using the approach described in the Experimental Section. With two fixed incident angles in the static neutron reflectivity experiment a large range of scattering vectors q_z is covered. In both curves the intensity modulation originating from the total nbc-PNIPAM film thickness is clearly visible. This is due to the high scattering length density (SLD) of the substrate and the gold top layer as compared to the polymer film. In addition, for the thick gold layer a weak long-wavelength modulation is due to the thickness of the gold layer itself. For the thin gold layer this is not resolved in the neutron reflectivity data.

The SLD profiles belonging to the fits shown in Figure 1 are displayed in Figure 2. Both profiles show a bilayer on top of the Si substrate. The nbc-PNIPAM layer agrees well with the SLD value expected for this polymer. An internal structure caused by the end-groups is not resolved due to a missing contrast between *n*-butyltrithiocarbonate and poly(*N*-isopropylacrylamide) in the neutron scattering experiment. As expected from the different sputter deposition times used in the preparation of the gold

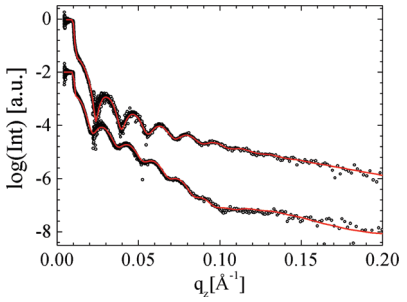

Figure 1. Neutron reflectivity data (dots) shown together with model fits (lines) for the 39.2 nm thick nbc-PNIPAM film coated with 0.4 nm nominal thick gold layer (top) and 5 nm nominal thick gold layer (bottom). The lower curve was shifted downwards for clarity.

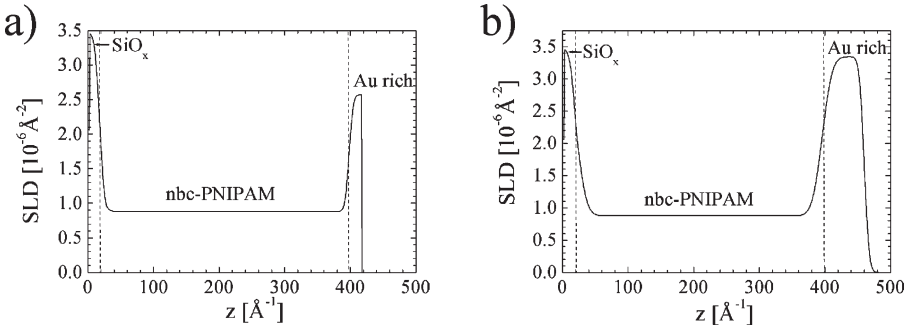

Figure 2. Resulting scattering length density (SLD) profiles of the two 39.2 nm thick nbc-PNIPAM films coated with a (a) 0.4 nm nominal thick gold layer and (b) 5 nm nominal thick gold layer.

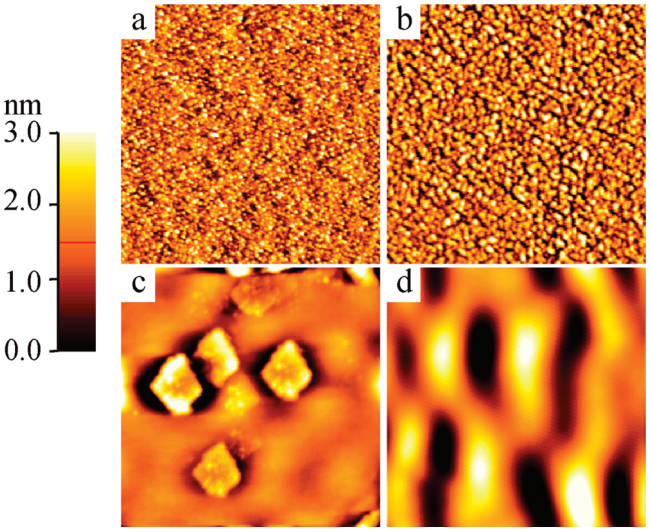

Figure 3. Topography AFM images of the bilayer films: (a, c) thin and (b, d) thick gold layer samples show different morphologies (a, b) before being subjected to water vapor atmosphere and (c, d) after the temperature jump experiments. The scan size is $1 \times 1\ \mu m^2$ for all AFM images. The structure height increases with the brightness of the structures in the images. The height scale bar range is 0−3 nm.

Scheme 1. Schematic Side View of the Bilayer Films Obtained by Sputter Deposition of Gold on nbc-PNIPAM Films: (Left) 0.4 nm Nominal Gold Layer Thickness and (Right) 5 nm[a]

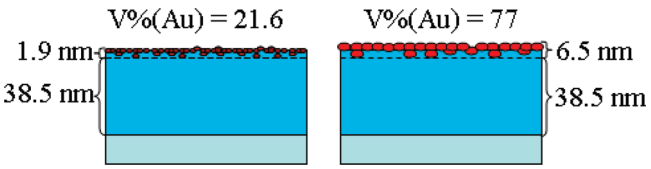

[a] For clarity of the presentation the *x*- and *y*-axes are not drawn to scale.

layers, the gold layers show the desired difference in thickness (nominal values 0.4 versus 5 nm). However, the nominal thicknesses are of course not recovered due to the complex process of gold deposition on the polymer material.[60] Moreover, the SLD values of the gold layers are smaller as compared to bulk gold and depend on the thickness. In case of the thin layer, a smaller SLD value is present as compared to the thick one. The thin gold layer extends over 1.9 nm and has a low amount of only 21 vol % gold. The thick gold layer spreads over 6.5 nm with 77 vol % gold. Thus, both gold layers exhibit an extension along the surface normal which exceeds the nominal value by 1.5 nm. From the profile it is obvious that gold diffuses into the nbc-PNIPAM surface region and that the gold surface is less flat as compared to the pure nbc-PNIPAM film surface (without gold deposition). Scheme 1 visualizes the corresponding structure of both films. It includes already information from the atomic force microscopy (AFM) measurements about the lateral surface structure of the gold films.

Whereas neutron reflectivity is sensitive to the structural information being projected onto the surface normal, AFM accesses lateral information.[61] AFM data are shown for $1 \times 1\ \mu m^2$ scan size. As sketched in Scheme 1 and shown by the AFM data presented in Figure 3, the thin gold film consists of small sized, (viewed from top) round-shaped gold grains, whereas the thick gold film shows larger gold grains. A round shape of the clusters is expected from the nonwetting behavior of gold on polymer surfaces.[61,62] Consequently, a 3D cluster growth (Volmer−Weber growth) is preferred over a 2D layer-by-layer growth (Frank−Van der Merwe growth) expected for the wetting

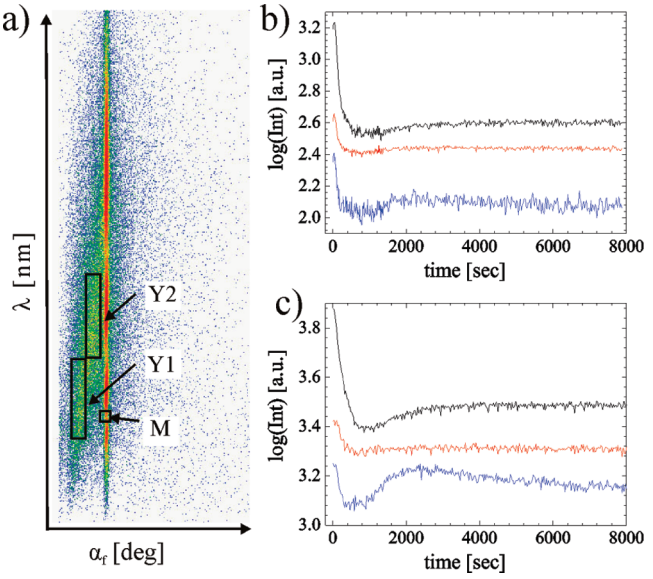

Figure 4. (a) Representative 2D detector pattern of the scattered intensity displayed in the wavelength λ to exit angle α_f presentation. The black boxes mark the areas integrated for the analysis of diffuse scattering. Intensities integrated over the areas M (top), Y1 (middle), and Y2 (bottom) (as explained in the text) are shown as a function of time for the (b) thick and (c) thin gold layer sample.

case. In the thin gold film the gold structures have a mean size of 25 nm and on the thick gold film this value is increased to 55 nm. Such increase of the gold structure with increasing gold layer thickness is in agreement with the typical growth behavior of gold on polymer surfaces.[60] For both samples the gold clusters have grown to a size in which the mean diameter is close to the mean correlation distance between two clusters; i.e., the clusters are in close contact with each other. Therefore, both, the thin and the thick gold film, belong to the coarsening stage of gold on polymer as described in ref 60. In this stage, coalescence is no longer dependent on migration, and the clusters grow rapidly in size. The same holds for the distance and the thickness. A detailed investigation of the growth behavior of gold on nbc-PNIPAM is beyond the scope of this article. Important is that both gold layers are closed layers with a grain morphology.

4. Results and Discussion of Switching Kinetics

The equilibrated bilayer films are exposed to saturated (deuterated) water vapor atmosphere in a custom-made vapor chamber. At the initial temperature of 23 °C, nbc-PNIPAM is below its LCST and thus the films are swollen with water.[63−67] The swelling kinetics and the cycling necessary to reach equilibrated films are described in the next section. Here we consider films which have reached an equilibrium regarding the swelling in water vapor atmosphere. With a temperature jump above the LCST the switching kinetics are determined for both gold layer thicknesses. We chose a jump to 40 °C because for thin nbc-PNIPAM films the LCST is significantly more spread out in temperature as compared to solutions.[38] For 39 nm nbc-PNIPAM films, a LCST at 29 °C is determined.[38]

Because of the use of deuterated water, we have good contrast conditions in the neutron reflectivity experiment and can follow the temperature jump with a high time resolution.

In Figure 4a, a representative 2D detector pattern of the scattered intensity (displayed as a function of wavelength λ and the exit angle α_f) is shown. Because off-specular neutron intensities are significantly lower than the specular ones, a detailed analysis of intensity as a function of lateral scattering vector component q_x is impossible for the kinetic data. The necessary

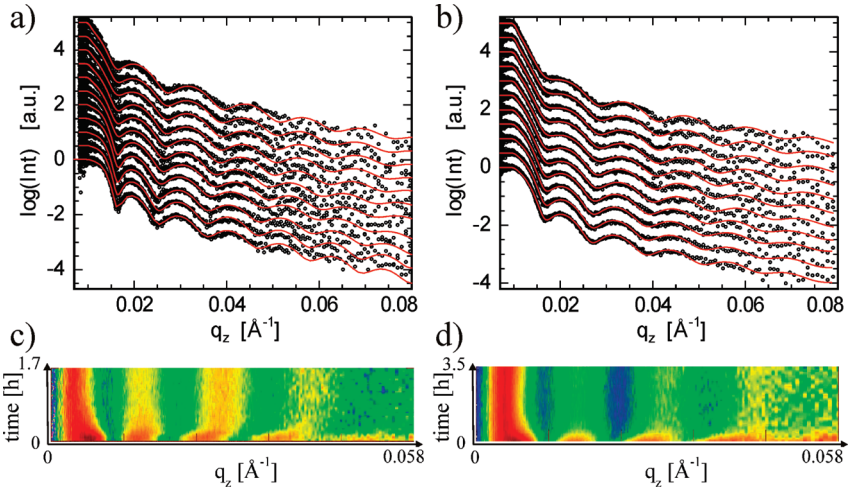

Figure 5. Comparison of the kinetics of the temperature jump of the (a, c) thick and (b, d) thin gold layer sample. In parts a and b, the measured reflectivities (dots) are shown with the fits to the data (lines). The curves are shifted along the *y*-axis for clarity of the presentation. Parts c and d are mappings of the measured specular neutron reflectivity versus time. The differences in colors show the differences in scattered intensities (red is high intensity, blue is low intensity).

improvement of statistics is achieved by an integration of the off-specular intensities. Thus, to keep the very high time resolution (14 or 24 s between successive neutron reflectivity curves) of the scattering experiment and to account for the kinetic changes of the films due to the temperature jump, an integration of intensities is performed in reciprocal space rather than in the time domain (by an increase of the counting time). The black boxes in Figure 4a mark selected regions in the intensity, which are used for the integration and further analysis: The integration region of off-specular scattered intensities are for the Yoneda peak intensities of deuterated material (Y1) and protonated material (Y2), respectively. For comparison the specularly reflected intensity (M) is integrated in a minimum of the reflectivity as well.

Parts b and c of Figure 4 show the time evolution of specular reflectivity (M), and off-specular reflectivities (Y1, Y2) for the temperature jump. Because of the jump above the LCST deuterated water is repelled from the nbc-PNIPAM films[66] and the SLD of the films decreases. This causes a decrease of the reflected intensity and a shift of the position of the total reflection edge toward a larger λ values. Accordingly, the intensity in the region M decreases with repelling of D_2O. Because of a loss of contrast the off-specular intensities Y1 and Y2 decrease both with time as well. In the swollen state D_2O had selectively diffused into parts of the film causing this contrast which upon extraction of D_2O gets lost. However, parts b and c of Figure 4 show that the decay is not monotonic and the overall behavior is more complex.

A more detailed analysis of the kinetics of the temperature jump is achieved by fitting the individual neutron reflectivity curves.[56,57] In these fits the bilayer sample is modeled with a main nbc-PNIPAM layer and a second gold-rich top-layer in agreement with the findings from the static samples and the AFM investigation.

Figure 5 shows a selection of fitted neutron reflectivity curves for both gold layer film thickness and a two-dimensional intensity presentation (mapping) of these specular intensities for both temperature jump experiments.

For both films the critical angle of total external reflection shifts toward smaller values of the scattering vector component q_z and the overall reflected intensity decreases. Both observations result from D_2O which is repelled out of the nbc-PNIPAM film.[37] Moreover, the wavelength of the intensity oscillations increases with time which shows that the films both get thinner. From a comparison of parts c and d of Figure 5, it is notable that the sample with the thin gold layer reacts faster to the temperature jump as compared to the thick gold layer. Parameters extracted from the fit to the reflectivity data are shown in Figure 6 as a function of time. There are four variables of each curve used for fitting: The thickness d and the SLD value n of the main nbc-PNIPAM layer and the top gold-rich layer, respectively. From the changes in the SLD values, the D_2O volume fraction $V\%_{D_2O}$ of the film is calculated using

$$V\%_{D_2O} = \frac{n - n_1}{n_2 - n_1} \quad (1)$$

where n denotes the in situ probed SLD of the film, n_1 the initial SLD of the dry film, and n_2 the SLD of D_2O. In Figure 6, the time evolution of the D_2O volume fraction $V\%_{D_2O}$ of the main layer and the top layer are presented, respectively.

The temperature increase in the bilayer sample is shown in Figure 6a. The temperature sensor was placed in the back of the substrate and the temperature was measured in situ. Afterward, the temperature measurement was repeated ex situ to make sure it is reproducible. The rate of temperature increasing was controlled and limited by the thermobath and also strongly influenced by the substrate and the sample as neither the Si substrate nor the polymer is a good heat conductor. After 110 s the LCST of 29 °C is reached (marked by the dashed line). The response of the thick gold layer film is presented in Figure 6, parts b and c. Because the thick gold layer contains 77 vol % gold, it remains unchanged during the temperature jump and is not displayed in Figure 6. The nbc-PNIPAM film (main layer) below the thick gold layer reacts with a decrease of its water content from 38 to 24 vol %. This is accompanied by a decrease in the relative film thickness d/d_{dry} from 1.27 to 1.10. The characteristic time constant for this water release is 280 s. However, surprisingly this decrease is followed by a slight relaxation back to higher water content and larger film thickness (27 vol % and 1.13). The time constant of this relaxation is larger with 900 s. The observed two-step process may be introduced by the asymmetric confinement of the nbc-PNIPAM film, which is sandwiched between a solid silicon support and a gold layer. Already from the integrated intensities presented in Figure 4, such a two step process was visible. Therefore, the temperature jump causes the nbc-PNIPAM film to collapse and afterward slowly rearrange into a different structure. In the relaxation a small amount of the surrounding water is taken up again and correspondingly the film relaxes to a larger film thickness as compared to the collapse.

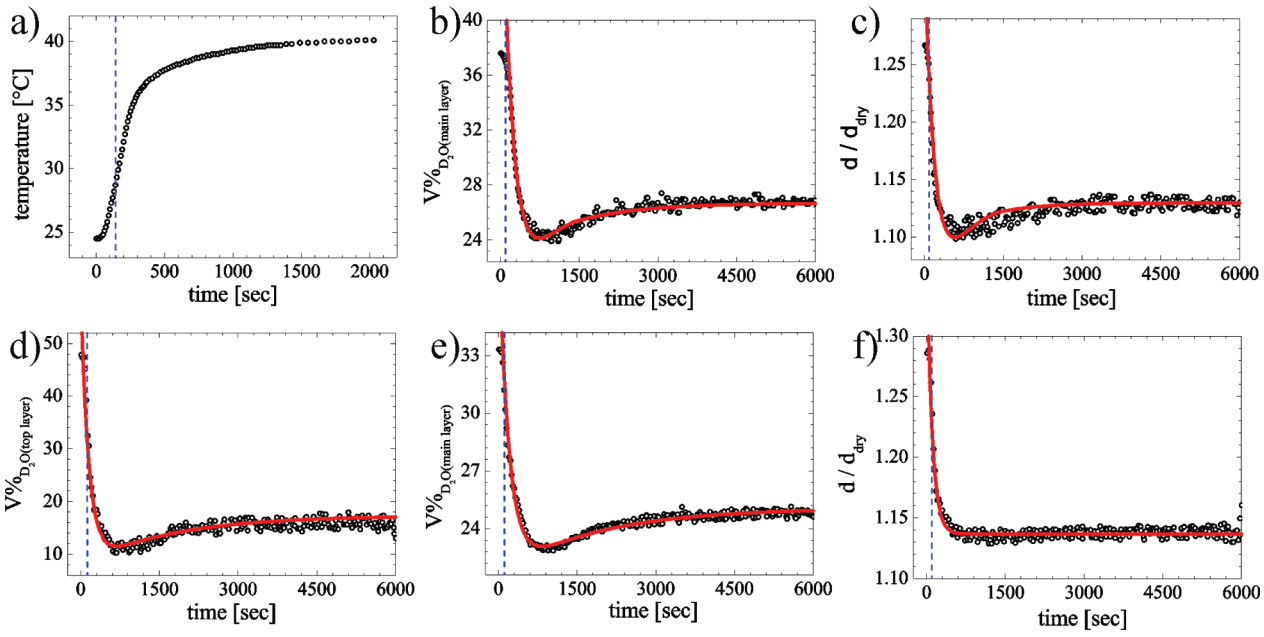

Figure 6. Switching kinetics from 23 to 40 °C followed by neutron reflectivity: (a) temperature increases as a function of time in the film. Volume percentage of water (D_2O) in the main layer of the film is shown as a function of time (b) for the thick and (e) the thin gold layer. Time-dependent change of the film thickness d normalized by the initial dry film thickness d_{dry} (c) for the thick and (f) the thin gold layer. Volume percentage of water in the top layer of the film is shown as a function of time (d) for the thin gold layer. The LCST of the nbc-PNIPAM film is reached at a time marked by the dashed line in all images.

The solid lines in Figure 6 are model fits based on the gel swelling and shrinking model by Li and Tanaka.[68] In this model, swelling and shrinking follows first-order kinetics and is not considered to be a pure diffusion process. Recently, we used this model to describe the water storage in PNIPAM-based block copolymer films, which resist swelling.[37] Despite the initial stages of the temperature jump experiment reported here, the observed behavior can be explained within this model by assuming a first fast shrinkage process followed by a second (small) slow reswelling process. The initial stages will be influenced by the passing of the LCST and are thus not expected to match to such a simple model approach.

Comparing now the thick gold layer film behavior (top row images in Figure 6) with the one of the thin gold layer (bottom row images in Figure 6) some differences are obvious. In contrast to the thick film, for the thin gold film, the gold layer itself (top layer) changes its water content (see Figure 6d). This is caused by the small gold volume fraction (21.6 vol %) of this layer, which means that most of the layer is nbc-PNIPAM as well. The full film, main (nbc-PNIPAM) and top (gold and nbc-PNIPAM) part exhibit the same two-step characteristics as seen for the sample with a thick gold layer as well. However, the time constants are different. The nbc-PNIPAM film reacts much faster and the characteristic time constant of water release is decreased to 190 s, as compared to the sample with a thick gold layer on top. In contrast, the relaxation back has a larger time constant of 1800 s. In addition, for the thin gold layer sample the gold containing part reacts as well with a similar behavior. The characteristic time constant of water release is 120 s and the time constant of the relaxation processes is 1330 s, respectively. Because of the interaction with the PNIPAM in the top layer part a large amount of water is incorporated (48 vol %) before the temperature jump. The release is very strong and finally only 15 vol % is left. The nbc-PNIPAM layer behaves quite similar to the one with more gold on top and reduces its amount of water from 34 to 23 vol %. In the change of the relative film thickness d/d_{dry} the values reduce from 1.28 to 1.13, which is as well equal to the observation on the thick gold layer sample. However, the two-step process is not visible and the change in relative film thickness appears to be a simple release.

Looking into the changes such temperature jump had made to the gold layer surface, again AFM is used. Figure 3 compares the morphology of the samples after being switched back and dried. Very clearly, the gold surface morphology is altered by this switching process. The gold structure has coarsened to characteristic lateral structures of 200 nm (thin gold layer) and 230 nm (thick gold layer). Moreover, a crystalline appearing morphology is present and the initial spheres of gold have merged into ribbon-like structures. However, the average height of the gold clusters for both samples did not change, which has been confirmed by AFM (in micrometer scale of probed sample surface) and also by neutron reflectivity (in centimeter scale of probed sample surface). This phenomenon was also considered in the fitting of the kinetic data.

In comparison between both gold layer thicknesses, the thinner gold layer sample reacts faster and shows very similar switching characteristics of the main nbc-PNIPAM film regarding the total shrinkage d/d_{dry}. As a consequence, such type of asymmetrically confined bilayer film is better suited for applications related to nanoswitches.

5. Results and Discussion of Swelling Kinetics

Because the thin gold layer appears better suited for switching kinetics we investigate this bilayer sample regarding its swelling kinetics and aging as well in detail. For this purpose a fresh, dry, gold coated nbc-PNIPAM film with 0.4 nm nominal gold layer thickness is mounted into the custom-made vapor chamber in air, thermostated to 23 °C. The swelling and deswelling cycle protocol is detailed in the Experimental Section. The addition of D_2O marks the starting point of the swelling kinetics (time = 0). We performed 7 cycles and the deswollen sample is always reused in the subsequent cycle.

In Figure 7, the measured neutron reflectivity curves are displayed. These curves show that basically after each complete swelling and deswelling cycle the bilayer sample is unchanged. Small changes occur only in the nbc-PNIPAM layer (main layer).

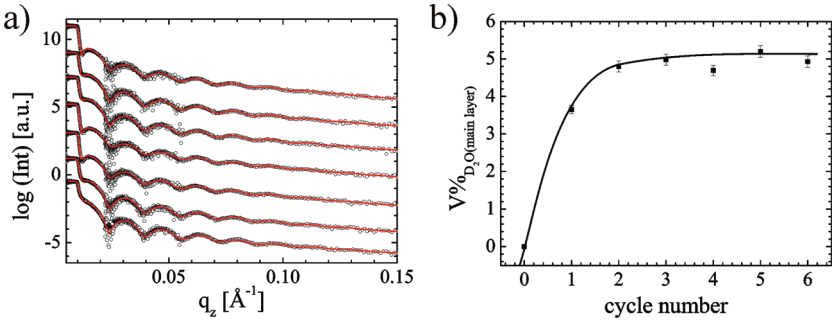

Figure 7. (a) Neutron reflectivity data (dots) shown together with model fits (lines) for the nbc-PNIPAM film coated with 0.4 nm nominal thick gold layer initially prepared (bottom curve) and measured after complete swelling−deswelling cycles (number of cycles increases from bottom to top). The curves are shifted for clarity. (b) Volume percentage of water in the main layer of the film as a function of cycle number.

Whereas the initially freshly used film contains no deuterated water, within the first two cycles the amount of D_2O increases to 5 vol %. In the following cycles this value remains constant. As reported for cyclic treatment of PNIPAM-based diblock copolymer films such behavior has two origins:[37] Water can be caused to remain by formation of strong chemical bonds between D_2O and PNIPAM molecules (bound water). Alternatively, H−D exchange occurring during water storage inside the film can give the impression of water that is not extractable. However, since only one H atom per PNIPAM unit (the one on the −CONH− group) can be replaced by a D atom, if we consider only H−D exchange and H-D exchange happening to all −CONH− moieties, the SLD of the main layer would be 1.5×10^{-6} Å^{-2} and the maximum SLD of the main layer of our dry sample after each cycle is only 1.15×10^{-6} Å^{-2}. Thus, it is difficult to conclude if the increase of SLD is fully due to the H−D exchange or is only partially due this reason. Of course, if there are strong chemical bonds between D_2O and PNIPAM, very similar bonds would exist for H_2O and PNIPAM, too. Hence, bound water could have existed already before exposure to D_2O. However, due to the small SLD of H_2O, it is hardly detectable by using neutrons.

As compared to the diblock copolymer sample (investigated in ref 30) no strong interface enrichment is found in the gold coated nbc-PNIPAM and the remaining amount is larger, perhaps due to the presence of the gold layer. Here, 5 vol % of D_2O is found in the nbc-PNIPAM film after it is cycled to equilibrium (see Figure 7b). Thus, the imposed asymmetric confinement changes the behavior as compared to a free polymer surface.

With grazing-incidence small-angle X-ray scattering (GISAXS) the cycled films are characterized concerning changes of the inner film structure. Figure 8 shows the vertical and horizontal cuts from the 2D GISAXS intensity. From the vertical cuts, we conclude that the perpendicular structure (correlated roughness, highlighted by the box in Figure 8a) is installed in the first cycles and later damped with increasing cycle number. For large wavelengths within the limited experimental resolution, the substrate and the polymer−vacuum interface are correlated.[69,70] So the long-ranged correlated nbc-PNIPAM film becomes better defined in the initial cycles and later independent in its surface structures from the substrate by slight roughening of the surface.[71,72] From the horizontal cuts, we find no influence of the cycling on the inner lateral film structure. In good agreement with the pure nbc-PNPAM films of different thickness,[38] the films investigated here show a weak peak in the intensity at large values of the scattering vector component q_y. Identical to microphase separated systems, the peak is a structure factor type information, showing that the thin nbc-PNIPAM films exhibit an internal structure. It resembles the distance between adjacent regions of hydrophobic *n*-butyltrithiocarbonate end groups in a PNIPAM matrix. The corresponding mean distance between domains of chain ends is 25 nm. Comparing this value with the micellar size

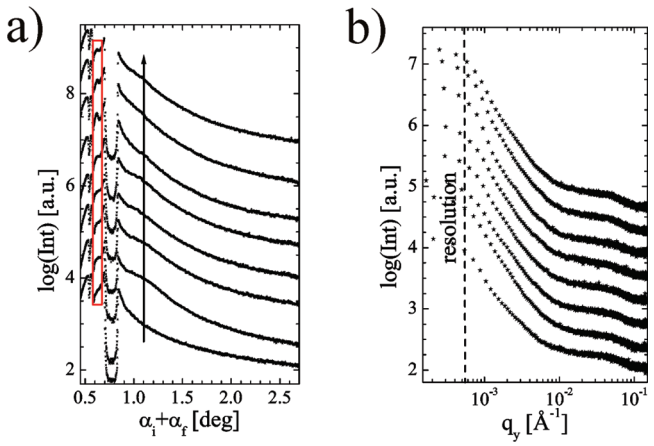

Figure 8. GISAXS data of nbc-PNIPAM films before swelling−deswelling cycle (bottom) and after seven swelling−deswelling cycles (subsequently shifted seven curves): (a) vertical cuts showing structures along the surface normal and (b) horizontal cuts (dots) showing in-plane structures.

detected in solution shows that the micelles are indeed bridged and entangled inside the film[38]. So GISAXS indicates no severe aging of the gold coated nbc-PNIPAM film which is important for applications.

During swelling and deswelling cycles in situ GISAXS measurements are impossible due to radiation damage occurring in swollen nbc-PNIPAM films.[37] As a consequence, we use again in situ neutron reflectivity and off-specular scattering to investigate the time dependence of the cycling.

As detailed in the previous section, the integration of selected areas from the collected 2D neutron data is a strong tool to characterize the time-dependent behavior. We chose the same boxes as shown in Figure 4. Therefore, Y1 refers to integration in a region of off-specular scattered intensities related to the Yoneda peak of deuterated material (see Figure 9b) and Y2 to protonated material (see Figure 9c), respectively. For comparison the specularly reflected intensity (M) is integrated in a minimum of the reflectivity as well (see Figure 9a).

Regarding the film thickness, despite the initial swelling, which behaves complex, in all swelling cycles the films swell by incorporation of water molecules. The initial swelling first requires a rearrangement of the molecules, which first causes even shrinkage before the film swells. In contrast, the incorporation of D_2O results in an increase of the diffuse scattering. The off-specular intensities Y1 and Y2 increase with time due to the buildup of a lateral structure inside the nbc-PNIPAM film because D_2O selectively diffuses into parts of the film which are not occupied by the hydrophobic end-groups.

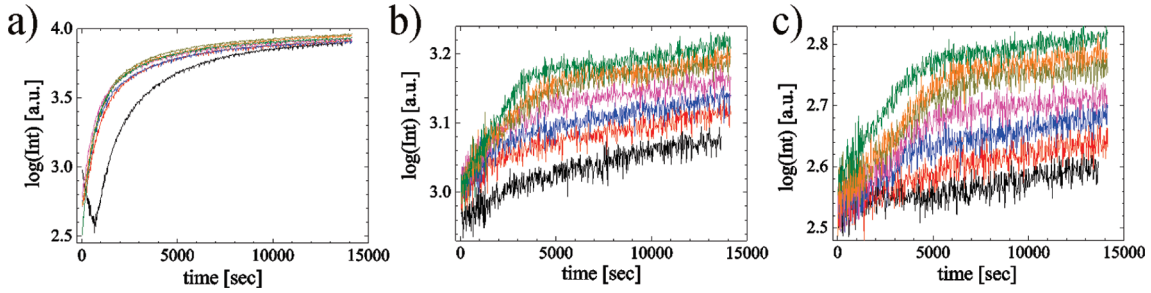

Figure 9. Integrated intensities of the 2D TOF neutron data with integration areas denoted (a) M, (b) Y1, and (c) Y2 showing the individual swelling behavior within the different cycles. From bottom to top the number of the cycle increases.

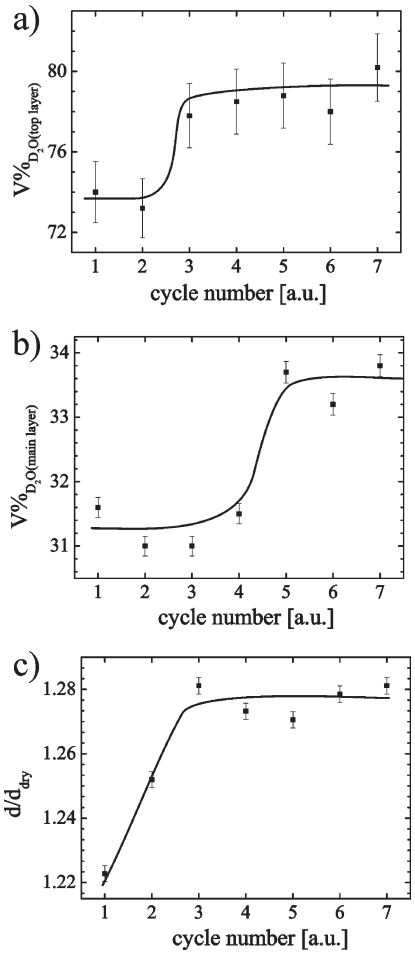

Figure 10. Maximum amount of water incorporated inside the (a) top part (gold and nbc-PNIPAM containing) and (b) main part (nbc-PNIPAM) at the end of each swelling cycle plotted as a function of the cycle number. (c) Cycle dependent change of the film thickness d normalized by the initial dry film thickness d_{dry}.

From a fit to the kinetic neutron reflectivity data, we extract the maximum amount of water which is incorporated inside the bilayer films and the degree of swelling (see Figure 10). All together these data show that the initially prepared film improves after some cycles and is able to swell more and to incorporate more water. Thus, again no aging is observed, which would reduce the film performance. After five cycles, equilibrium is reached. The degree of swelling, as well as the amount of incorporated water, is independent from the cycle number. In detail, the top part of the film, containing the gold, behaves differently from the main part which is pure nbc-PNIPAM. In good agreement with the switching experiment, more water molecules are incorporated in the top part as compared to the main film, due to the interaction with the gold.

Regarding the extracted parameters, the cycled sample after 7 cycles is in good agreement with the starting condition of the temperature jump experiment. In saturated water vapor atmosphere the relative film thickness d/d_{dry} is 1.28, the nbc-PNIPAM film (main layer) water content is 34 vol % and the top layer contains 80 vol % water (in Figure 5d a smaller value is observed due to the fast reaction of the top layer to the temperature jump).

6. Conclusion

We successfully prepare and characterize a thin hydrogel film confined between Si and gold, its response to changes of the temperature (jump from below LCST to above LCST) and swelling kinetics. Such asymmetrically confined hydrogel film can be understood as a simplified thin film sensor and nanoswitch which consists of the active (sensor) layer and a metal top-layer in thin film geometry. We use nbc-PNIPAM with a gold layer on top which is deposited by sputter deposition. From the comparison of the two different gold layer thicknesses used in this investigation (nominal 0.4 and 5 nm), the thinner one turned out to be better suited for the use in switching due to its faster response time. The structural characterization based on in situ neutron scattering shows that at least 5 swelling and deswelling cycles of the bilayer films are necessary to achieve an equilibrium film structure regarding the increase of the film thickness caused by the swelling and the amount of water stored in the film. In the initial stages, the films rearrange from the structure formed during the preparation. However, in the dry films, this is not reflected by a marked rearrangement of the inner microphase separation-like demixing of PNIPAM and its end-groups, but caused by a change of the gold layer morphology. As the water molecules mainly have to pass this gold layer it is obvious that such rearrangement will influence the swelling performance. Nevertheless, this process is not giving rise to a severe aging of the nbc-PNIPAM film.

The observed switching behavior due to a temperature jump above the LCST is not just a simple release of water molecules but a two step process. The water release and film shrinkage are followed by a relaxation of the molecules and a small secondary water uptake. Both processes are modeled within the swelling and deswelling model by Li and Tanaka.[68] Thus, the incorporation of water molecules is not a simple diffusion process as observed previously for PNIPAM-based block copolymer films. The imposed confinement might cause the observed two step process and the added gold layer might originate the relaxation process after water release.

With respect to applications, however, one has to consider that the changes in film thickness are small, both in the switching and cycling. This is caused, on the one hand by the small value of the total nbc-PNIPAM film thickness used in this investigation, and on the other hand, by constraints add to the system due to the top

gold layer. Pure nbc-PNIPAM films have shown a much stronger swelling if exposed to water vapor atmosphere.[38] Thus, a confined hydrogel film reacts more weakly as compared to a free surface film. Nevertheless, a thin gold layer is necessary for such applications to act as a contact material or as a capacitor. On the basis of the observations on block copolymer thin films with increased hydrophobic blocks which swell less if exposed to water vapor atmosphere,[37] the presented system appears to be quite optimized.

Acknowledgment. We thank A. Timmann for his help during the alignment of BW4 beamline at HASYLAB. Financial support by the DFG in the priority program SPP1259 (PA771/4, LA611/7, and MU1487/8) is gratefully acknowledged.

References and Notes

(1) Winnik, F. M. *Macromolecules* **1990**, *23*, 233.
(2) Schild, H. G. *Prog. Polym. Sci.* **1992**, *17*, 163.
(3) Tam, K. C.; Wu, X. Y.; Pelton, R. H. *J. Polym. Sci., Polym. Chem. Ed.* **1993**, *31*, 963.
(4) Tiktopulo, E. I.; Bychkova, V. E.; Ricka, J.; Ptitsyn, O. B. *Macromolecules* **1994**, *27*, 2879.
(5) Wu, C.; Zhou, S. *Macromolecules* **1995**, *28*, 8381.
(6) Wang, X.; Qiu, X.; Wu, C. *Macromolecules* **1998**, *31*, 2972.
(7) Pelton, R. *Adv. Colloid Interface Sci.* **2000**, *85*, 1.
(8) Maeda, Y.; Higuchi, T.; Ikeda, I. *Langmuir* **2001**, *17*, 7535.
(9) Stieger, M.; Richtering, W. *Macromolecules* **2003**, *36*, 8811.
(10) Kita, R.; Wiegand, S. *Macromolecules* **2005**, *38*, 4554.
(11) Lutz, J.-F.; Akdemir, Ö.; Hoth, A. *J. Am. Chem. Soc.* **2006**, *128*, 13046.
(12) Skrabania, K.; Kristen, J.; Laschewsky, A.; Akdemir, Ö.; Hoth, A.; Lutz, J.-F. *Langmuir* **2007**, *23*, 84–93.
(13) Bivigou-Koumba, A. M.; Görnitz, E.; Laschewsky, A.; Müller-Buschbaum, P.; Papadakis, C. M. *Colloid Polym. Sci.* **2010**, *288*, online first.
(14) Aoshima, S.; Kanaoka, S. *Adv. Polym. Sci.* **2007**, *210*, 169–208.
(15) *Stimuli-Responsive Water Soluble and Amphiphilic Polymers*; McCormick, C. L., Ed.; ACS Symposium Series 780; American Chemical Society: Washington, DC, 2001.
(16) Wei, H.; Cheng, S.; Zhang, X. *Prog. Polym. Sci.* **2009**, *34*, 893–910.
(17) Liu, R.; Fraylich, M.; Saunders, B. R. *Colloid Polym. Sci.* **2009**, *287*, 627–643.
(18) Cooperstein, M. A.; Canavan, H. E. *Langmuir* **2009**, *25*, doi: 10.1021/la902587p
(19) Lopez, G.; Chilkoti, A.; Atanassov, P.; Goparaju, V.: Stimuli responsive hybrid materials containing molecular actuators and their applications US patent 6491061B1, **2002.**
(20) Reese, C. E.; Mikhonin, A. V.; Kamenjicki, M.; Tikhonov, A.; Asher, S. A. *J. Am. Chem. Soc.* **2004**, *126*, 1493.
(21) Huber, D. L.; Manginell, R. P.; Samara, M. A.; Kim, B. I.; Bunker, B. C. *Science* **2003**, *301*, 352.
(22) Twaites, B. R.; de las Heras Alarcon, C.; Cunliffe, D.; Lavigne, M.; Pennadam, S.; Smith, J. R.; Gorecki, D. C.; Alexander, C. *J. Controlled Release* **2004**, *97*, 551.
(23) Park, Y. S.; Ito, Y.; Imanishi, Y. *Langmuir* **1998**, *14*, 910.
(24) Tanaka, T.; Nishio, I.; Sun, S. T.; Ueno-Nishio, S. *Science* **1982**, *218*, 67.
(25) Nuopponen, M.; Ojala, J.; Tenhu, H. *Polymer* **2004**, *45*, 3643.
(26) Hellweg, T.; Dewhurst, C. D.; Eimer, W.; Kratz, K. *Langmuir* **2004**, *20*, 4330.
(27) Zhang, W.; Zhou, X.; Li, H.; Fang, Y.; Zhang, G. *Macromolecules* **2005**, *38*, 909.
(28) Troll, K.; Kulkarni, A.; Wang, W.; Darko, C.; Bivigou Koumba, A. M.; Laschewsky, A.; Müller-Buschbaum, P.; Papadakis, C. M. *Colloid Polym. Sci.* **2008**, *286*, 1079.
(29) Lin, H.-H.; Cheng, Y.-L. *Macromolecules* **2001**, *34*, 3710–3715.
(30) Hietala, S.; Nuopponen, M.; Kalliomäki, K.; Tenhu, H. *Macromolecules* **2008**, *41*, 2627.
(31) Nykänen, A.; Nuopponen, M.; Hiekkataipale, P.; Hirvonen, S.-P.; Soininen, A.; Tenhu, H.; Ikkala, O.; Mezzenga, R.; Ruokolainen, J. *Macromolecules* **2008**, *41*, 3243.
(32) Nykänen, A.; Nuopponen, M.; Laukkanen, A.; Hirvonen, S.-P.; Rytela, M.; Turunen, O.; Tenhu, H.; Mezzenga, R.; Ikkala, O.; Ruokolainen, J. *Macromolecules* **2007**, *40*, 5827.
(33) Zhou, X.; Ye, X.; Zhang, G. *J. Phys. Chem. B.* **2007**, *111*, 5111.
(34) Jain, A.; Kulkarni, A.; Bivigou Koumba, A. M.; Wang, W.; Busch, P.; Laschewsky, A.; Müller-Buschbaum, P.; Papadakis, C. M. *Macromol. Symp.*, in press.
(35) Bivigou Koumba, A. M.; Kristen, J.; Laschewsky, A.; Müller-Buschbaum, P.; Papadakis, C. M. *Macromol. Chem. Phys.* **2009**, *210*, 565–578.
(36) Wang, W.; Metwalli, E.; Perlich, J.; Troll, K.; Papadakis, C. M.; Cubitt, R.; Müller-Buschbaum, P. *Macromol. Rapid Commun.* **2009**, *30*, 114.
(37) Wang, W.; Metwalli, E.; Perlich, J.; Papadakis, C. M.; Cubitt, R.; Müller-Buschbaum, P. *Macromolecules* **2009**, *42*, 9041.
(38) Wang, W.; Troll, K.; Kaune, G.; Metwalli, E.; Ruderer, M.; Skrabania, K.; Laschewsky, A.; Roth, S. V.; Papadakis, C. M.; Müller-Buschbaum, P. *Macromolecules* **2008**, *41*, 3209.
(39) Pelton, R. *Adv. Col. Interface Sci.* **2000**, *85*, 1.
(40) Murray, M. J.; Snowden, M. J. *Adv. Col. Interface Sci.* **1995**, *54*, 73.
(41) Karg, M.; Pastoriza-Santos, I.; Rodriguez-Gonzalez, B.; von Klitzing, R.; Wellert, S.; Hellweg, T. *Langmuir* **2008**, *24*, 6300.
(42) Schmidt, S.; Motschmann, H.; Hellweg, T.; von Klitzing, R. *Polymer* **2008**, *49*, 749.
(43) Tsuji, S.; Kawaguchi, H. *Langmuir* **2005**, *21*, 8439.
(44) Serpe, M. J.; Jones, C. D.; Lyon, L. A. *Langmuir* **2003**, *19*, 8759.
(45) Serpe, M. J.; Lyon, L. A. *Chem. Mater.* **2004**, *16*, 4373.
(46) You, Y.-Z.; Zhou, Q.-H.; Manickam, D. S.; Wan, L.; Mao, G.-Z.; Oupicky, D. *Macromolecules* **2007**, *40*, 8617.
(47) Tamirisa, P. A.; Hess, D. H. *Macromolecules* **2006**, *39*, 7092.
(48) Guenther, M.; Kuckling, D.; Corten, C.; Gerlach, G.; Sorber, J.; Suchaneck, G.; Arndt, K.-F. *Sensors and Actuators B-Chem.* **2007**, *126*, 97.
(49) Guenther, M.; Gerlach, G.; Corten, C.; Kuckling, D.; Sorber, J.; Arndt, K. -F. *Sensors Actuators B: Chem.* **2008**, *132*, 471.
(50) Kuckling, D. *Colloid Polym. Sci.* **2009**, *287*, 881.
(51) Barbey, R.; Lavanant, L.; Paripovic, D.; Schüwer, N.; Sugnaux, C.; Tugulu, S.; Klok, H.-A. *Chem. Rev.* **2009**, *109*, 5437.
(52) Diamanti, S.; Arifuzzaman, S.; Genzer, J.; Vaia, R. A. *ACS Nano* **2009**, *3*, 807.
(53) Müller-Buschbaum, P. *Eur. Phys. J. E* **2003**, *12*, 443.
(54) Couet, S.; Diederich, T.; Schlage, K.; Röhlsberger, R. *Rev. Sci. Instrum.* **2008**, *79*, 093908.
(55) Cubitt, R.; Fragneto, G. *Appl. Phys. A: Mater. Sci. Process.* **2003**, *74*, 329.
(56) Nelson, A. *J. Appl. Crystallogr.* **2006**, *39*, 273.
(57) Parrat, L. G. *Phys. Rev. B* **1954**, *95*, 359.
(58) Roth, S. V.; Döhrmann, R.; Dommach, M.; Kuhlmann, M.; Kröger, I.; Gehrke, R.; Walter, H.; Schroer, C.; Lengeler, B.; Müller-Buschbaum, P. *Rev. Sci. Instrum.* **2006**, *77*, 085106.
(59) Müller-Buschbaum, P. *Anal. Bioanal. Chem.* **2003**, *376*, 3.
(60) Kaune, G.; Ruderer, M. A.; Metwalli, E.; Wang, W.; Couet, S.; Schlage, K.; Röhlsberger, R.; Roth, S. V.; Müller-Buschbaum, P. *ACS Appl. Mater. Interfaces* **2009**, *1*, 353.
(61) Müller-Buschbaum, P.; Bauer, E.; Wunnicke, O.; Stamm, M. *J. Phys.: Condens. Matter* **2005**, *17*, S363.
(62) von Bechtolsheim, C.; Zaporojtchenko, V.; Faupel, F. *Appl. Surf. Sci.* **1999**, *151*, 119.
(63) Akiyoshi, K.; Kang, E.-C.; Kurumada, S.; Sunamoto, J.; Principi, T.; Winnik, F. M. *Macromolecules* **2000**, *33*, 3244–3249.
(64) Kujawa, P.; Winnik, F. M. *Macromolecules* **2001**, *34*, 4130.
(65) Kujawa, P.; Segui, F.; Shaban, S.; Diab, C.; Okada, Y.; Tanaka, F.; Winnik, F. M. *Macromolecules* **2006**, *39*, 341–348.
(66) Koga, T.; Tanaka, F.; Motokawa, R.; Koizumi, S.; Winnik, F. M. *Macromolecules* **2008**, *41*, 9413.
(67) Meng, Z.; Hendrickson, G. R.; Lyon., L. A. *Macromolecules* **2009**, *42*, 7664.
(68) Li, Y.; Tanaka, T. *J. Chem. Phys.* **1990**, *92*, 1365.
(69) Müller-Buschbaum, P.; Gutmann, J. S.; Lorenz, C.; Schmitt, T.; Stamm, M. *Macromolecules* **1998**, *31*, 9265.
(70) Müller-Buschbaum, P.; Gutmann, J. S.; Kraus, J.; Walter, H.; Stamm, M. *Macromolecules* **2000**, *33*, 569.
(71) Mahltig, B.; Walter, H.; Harrats, C.; Müller-Buschbaum, P.; Jerome, R.; Stamm, M. *Phys. Chem. Chem. Phys.* **1999**, *1*, 3853.
(72) Mahltig, B.; Müller-Buschbaum, P.; Wolkenhauer, M.; Wunnicke, O.; Wiegand, S.; Gohy, J. F.; Jérôme, R.; Stamm, M. *J. Colloid Interface Sci.* **2001**, *242*, 36.